Macromolecular Research

Article

DOI 10.1007/s13233-018-6121-1

www.springer.com/13233 pISSN 1598-5032 eISSN 2092-7673

Fabrication of 3D Self-Assembled Nonmulberry *Antheraea Mylitta* (tasar) Fibroin Nonwoven Mats for Wound Dressing Applications

Chandra Mohan Srivastava[1,2]
Roli Purwar*[,2]

[1] Centre for Polymer Technology, Amity School of Applied Science, Amity University, Gurgaon, Haryana-122413, India
[2] Department of Applied Chemistry, Delhi Technological University, Shahbad Daulatpur, Bawana Road, Delhi-110042, India

Received November 9, 2017 / Revised March 21, 2018 / Accepted March 31, 2018

Abstract: This research was focused on the two-step regeneration of *Antheraea mylitta* (tasar) fibroin in the form of electrospun 3D self-assembled nanofibrous nonwoven mats using ionic liquid and formic acid/$CaCl_2$.The self-assembled structure of tasar nanofibrous nonwoven mats was dependent on the silk fibroin concentration and spinning voltage. The secondary conformation of tasar fibroin protein before and after electrospinning was analyzed by Fourier transformation infrared spectroscopy. The morphology of the nanofibrous mat was studied by scanning electron microscope. The self-assembled 3D tasar nonwoven nanofibrous construct was a highly porous and spongy structure with high water absorption and water vapor transmission. Highly porous 3D self-assembled tasar nonwoven nanofibrous construct favored good growth and proliferation of L929 skin fibroblast cells. Based on these properties, 3D self-assembled tasar nonwoven nanofibrous construct is a promising material for skin tissue engineering and wound dressing applications.

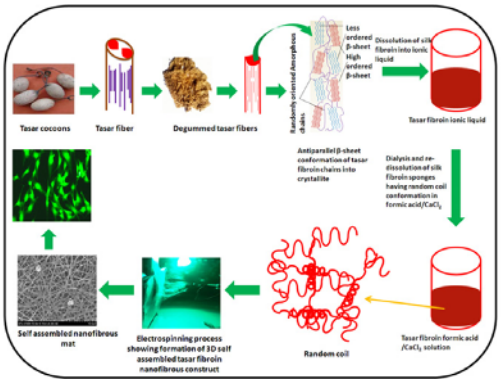

Keywords: tasar fibroin, self-assembled nanofibrous mat, electrospinning, skin tissue engineering.

1. Introduction

Wound healing is a very complex phenomenon involving several integrated biological and molecular events such as cell migration, proliferation, extracellular matrix (ECM) deposition and remodeling[1] that may get altered under certain pathophysiologic and metabolic conditions.[2] The ideal wound dressing should have following properties such as good exudates absorption ability, provide moist environment, biocompatible, biodegradable, porosity, non-adherent nature, water vapor and gas permeability, soft and comfort and adequate mechanical properties. There are different types of wound dressings available commercially, namely foam, hydrocolloids, alginate, hydrogel, iodine and silver impregnated dressings. The choice of particular wound dressing must be on the basic nature of wound. Nanofibrous mats have been successfully utilized in wound management. The highly porous architecture of nanofibrous mats allows the materials to absorb the large amount of exudates, promote higher adherence, growth, proliferation and migration of cells. This is achieved due to the high surface area, roughness, permeation of gases and water vapors as well as ease passage of metabolites & nutrients which is essential for the growth of neo-tissue and regeneration of damaged tissues. Due to high surface area, porosity and structural similarity of natural extracellular matrix, these cells seeded nanofibrous scaffolds may be good substitute of autografts, allografts and xenografts.[3,4]

Electrospinning is a straightforward and proficient technique to produce the polymeric nanofibers with size ranging from submicron to nano range. The nanofibrous mats produced by electrospinning have very high surface area and microporous architecture. This makes them an ideal matrix for cells growth and its proliferation.[5] Recently, electrospinning is used for producing self-assembled architectures for biomedical applications.[6,7] The concept of self-assembled nanofibers yarn by electrospinning was given by Okuzaki *et al.*[8] The presence of the low molecular weight salt in the spinning solution was considered as the main prerequisite for initiation of the self-organization process. The diameter of the yarns was also depended on the salt and polymer concentration. In general, the self-assembled nanofiber yarns are not stable and collapsed once the high electric field is removed. This generates a highly porous and spongy 3D nanofibrous matrix.[9]

Tasar fibroin protein has been explored as potential biomaterial due to its very good biocompatibility, controlled biodegradability and tuned mechanical properties.[10] The higher biocompatibility of nonmulberry tasar silk fibroin protein over mulberry silk fibroin protein is due to the presence of tripeptide sequences (Arg(R)-Gly(G)-Asp(D), which promotes proliferation of fibroblast and remodeling of epithelial tissues.[6] Nanofibrous 2D

Acknowledgments: Authors would like to thank the Council of Scientific and Industrial Research (CSIR-HRDG) for providing SRF grant (08/133(0009)/2014-EMR-I). Authors acknowledge Dr. Amit Misra and co-worker Mr. Deepak Sharma, CSIR-CDRI Lucknow for providing lab facilities to carry out cytocompatibility tests.

***Corresponding Author:** Roli Purwar (roli.purwar@dce.edu)

architectures from tasar gland fibroin and its blend have been prepared by various researchers.[11,12] The highly porous tasar nanofibrous mats have been prepared through electrospinning by dissolving the tasar gland protein into formic acid/chloroform (60:40 v/v). These mats showed higher adherence and proliferation of mesenchymal stem cells as compared to mulberry and gelatin nanofibrous mats.[11] Bhattacharjee *et al.*[12] fabricated tasar gland fibroin proteins and polyvinyl alcohol blends based 2D nanofibrous mats using electrospinning for bone tissue engineering applications. Eri/tasar blends based nanofibrous 2D mats showed higher mechanical integrity and very good adherence, proliferation and differentiation of human mesenchymal stem cells over mulberry and gelatin nanofibrous mats.[12] Zhao *et al.*[13] developed self-assembled electrospun mulberry silk nanofibers for biomedical applications. To the best of our knowledge based on literature search, electrospun self-assembled 3D architecture from nonmulberry silk especially from tasar fibroin obtained from cocoon has not been reported yet.

The present work was focused on the fabrication and characterization of self-assembled tasar silk fibroin nanofibrous nonwoven 3D constructs using electrospinning. The strong hydrophobic interaction in crystalline region of tasar fibroin protein makes it insoluble in most of solvents in which mulberry silk fibroin dissolve. Two steps dissolution process was adopted for preparation of electrospinning dope solution. The tasar fibroin was first dissolve in the 1-butyl-3-methylimidazolium acetate ionic liquid. By this process tasar fibroin polymer chains were converted into random coil conformation from β-sheet. The random coil tasar fibroin protein was extracted from the ionic liquid solution by dialysis and freeze drying. The obtained tasar fibroin protein was easily dissolved in formic acid/$CaCl_2$ to prepare dope solution for electrospinning. By varying the process parameters of electrospinning, self-assembled architecture of tasar fibroin was obtained and characterized. A schematic diagram for preparation of self-assembly tasar nanofibrous construct is shown in Figure 1.

2. Experimental

2.1. Materials

The tasar cocoons were procured by Central Silk Board, Sonbhadra, U.P, India. The ionic liquid 1-butyl-3-methylimidazolium acetate was procured from Sigma Aldrich. The L929 mouse skin fibroblast cells were purchased from National Centre of Cell Science, Pune. All other chemicals used in this study were purchased from Sigma-Aldrich till it is specified.

2.2. Preparation of tasar silk fibroin solution

Degumming and dissolution of tasar cocoon were performed as per protocol we have used in our previous research.[14] Briefly, tasar silk fibroin cocoons were cut in small pieces (4-8 mm), washed with distilled water and boiled in 0.02 M $NaHCO_3$ for

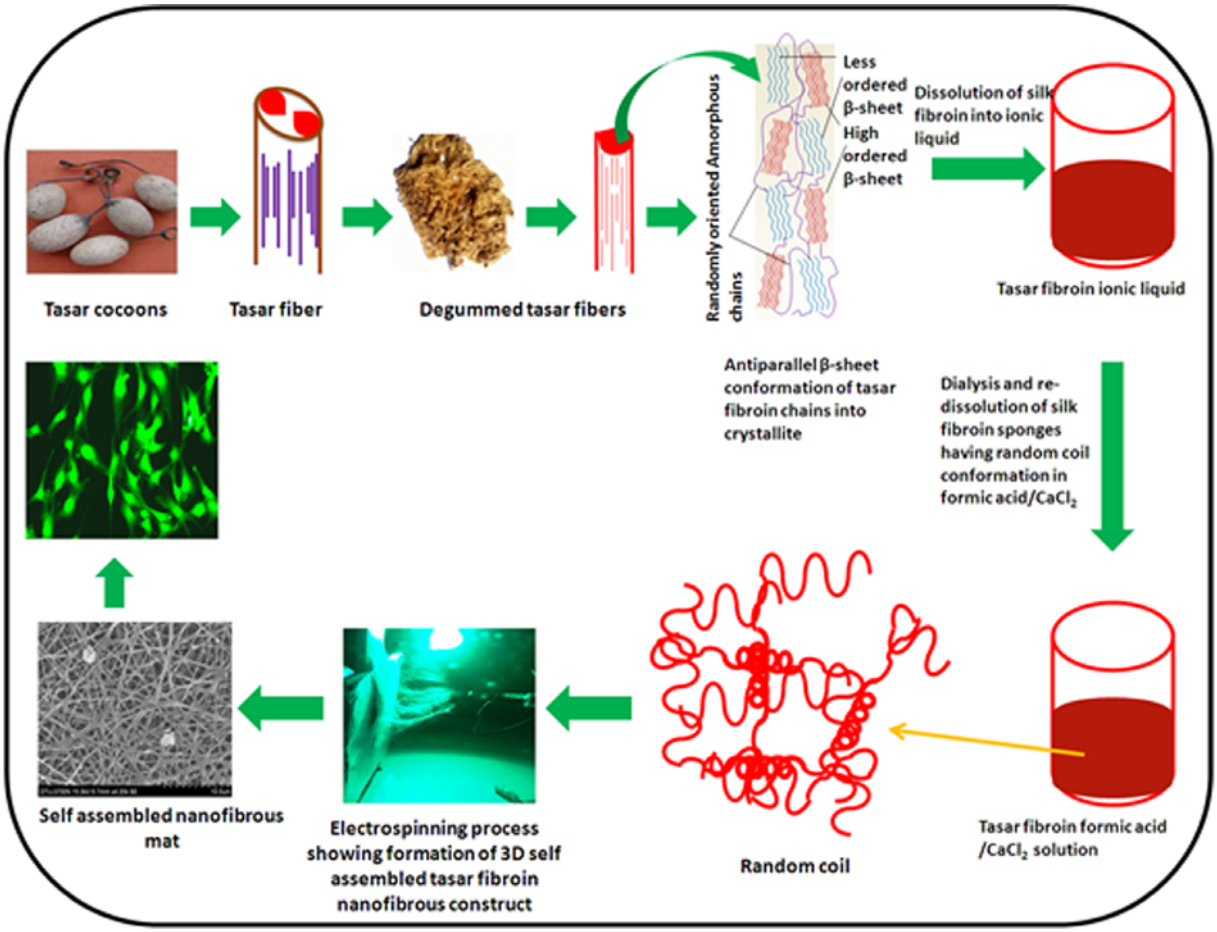

Figure 1. Schematic representation for the preparation of self-assembled tasar nanofibrous mat.

1 h to remove hot water soluble sericin protein. The degummed tasar fibroin fibers were washed again with distilled water to remove any traces of salts and dried in oven. Dried tasar fibroin fibers were dissolved in the ionic liquid; 1-butyl-3-methylimidazolium acetate under inert atmosphere at 95 °C for 2 h under continuous stirring. The tasar ionic liquid solution was dialyzed against distilled water using dialysis flask (Thermo scientific Slide-A-Lyzer) for 3 days to obtain aqueous tasar silk fibroin protein solution. The molecular weight of aqueous tasar fibroin solution as determined by SDS-PAGE was found to be 390 kDa. Tasar silk fibroin powder was obtained using freeze drier. This tasar silk fibroin powder was again dissolved in the 98% formic acid/$CaCl_2$ (2% w/v) solution for electrospinning with concentration of 10, 15, and 20% w/v. More than 20% w/v silk/formic acid/$CaCl_2$ solution is difficult to prepare and process in electrospinning machine due to very high viscosity.

2.3. Preparation of 3D self-assembled tasar silk fibroin nanofibrous mat by electrospinning

Tasar silk fibroin formic acid solution was fed through 10 mL plastic syringe having needle with tip diameter of 0.2 mm. Electrospinning was performed on Royal electrospun machine at different voltages (15 and 25 kV) and concentration (10, 15 and 20%) in order to obtain self-assembled structure. The prepared nanofibrous mats were coagulated in 80% (v/v) methanol for 30 min to remove residual formic acid and repeatedly washed with distilled water and dried in oven. Each sample has been assigned a name. For example, if the sample had 10% tasar fibroin concentration, name of the sample was given 10% STNF.

2.3.1. Fourier transform infrared spectroscopy

The conformational changes in tasar fibroin protein after dissolution as well as after regeneration in the form of 3D nanofibrous construct (STNF) was determined by ATR-FTIR (Thermo Scientific Nicolet 380 Spectrometer, Japan) in reflection mode at 4 cm^{-1} resolution using 64 scans in the spectral range 2000 to 800 cm^{-1}.

2.3.2. Morphological characterization

Different self-assembled 3D nanofibrous mats were sputter coated with gold and analyzed by scanning electron microscope (Hitachi 3700 N). Fiber diameter was calculated by Image J software by analyzing at least 30 fibers from 10 images randomly.

2.3.3. Mechanical testing

The mechanical integrity of samples was analyzed by Universal Testing Machine (Instron-2700) in tension mode as per ASTM D 882-02. The samples were prepared as per ASTM D 882. Briefly, the samples were cut into strips with dimensions of 70×10×3 mm and tabbed 10 mm at both end with gauge length of 50 mm. The tabbed samples were fixed at the jaw of tensile tester and stretched at the strain rate of 10 mm/min.[14] The samples were tested in triplicate and their stress-strain curves were recorded.

2.3.4. Porosity, pore size, and surface roughness

Porosity of self-assembled nanofibrous construct (20% STNF) was measured by liquid displacement method.[15] In this particular experiment we used hexane as displacement liquid because it easily permeates into sample through interconnected pores without any remarkable shrinkage and swelling. For measurements, a rectangular piece of sample was immersed in graduated cylinder having known volume of hexane (V_1) for 10 min. The volume of hexane with immersed sample was recorded (V_2). The residual volume of hexane in graduated cylinder after removal of samples was noted as (V_3). The percent porosity of the samples was calculated by the equation:

$$\varepsilon(\%) = [(V_1\text{-}V_3)/(V_2\text{-}V_3)]\times 100 \quad (1)$$

Surface topography, porosity and nanophase surface roughness of nanofibrous samples were evaluated by Atomic force microscope (Park XE-100) equipped with a V shape of silicon nitride cantilever connected with spring having spring constant 40 N/m in contact mode. The topography and surface roughness of the samples were determined at ambient temperature by scanning the area of 2×2 μm. The roughness of samples was measured as arithmetic average (R_a) that represents the average deviation of roughness values. The average pore size was calculated using Image J software by measuring at least 10 pores.[14,16]

2.3.5. Water uptake

Water uptake behavior of nanofibrous samples was determined by the standard protocol with little modification.[17] Briefly, the dried samples were cut in square shape (20 mm × 20 mm) and weighed. The samples were dipped in distilled water and incubated at 37 °C. At predetermined time, the samples were taken out and gently bolt with tissue paper to remove any water remained at the surface. The weight of swollen samples was recorded at different time point till saturation has to be maintained. Percent water uptake was determined by the equation given below:

$$\%\ \text{Water uptake} = \frac{\text{Wet Weight-Dry Weight}}{\text{Dry Weight}}\times 100\% \quad (2)$$

2.3.5. Water vapor transmission rate (WVTR)

WVTR of self-assembled nanofibrous mat was measured as per ASTM D 1653 standard with some modifications.[18] Briefly, a plastic cup having a known amount of distilled water was sealed carefully with 9.5 cm^2 nanofibrous films. The nanofibrous film sealed assembly was weighed and kept in the environment of 36±0.5 °C temperature and 40±2% relative humidity for 24 h, and then weighed again. Water vapor transmission rate for nanofibrous construct was calculated by the equation and expressed as g/m^2/day:

$$\text{WVTR} = \frac{W_a - W_b}{A\times 24} \quad (3)$$

where, W_a and W_b represent the weight of assembly before and after 24 h of water evaporation, respectively, and A represents area of sealed samples from which effective transmission occur. The experiment was performed in triplicate and results are given as average.

2.3.7. Biocompatibility tests

2.3.7.1. Cell Culture

The L929 skin fibroblast cell line was purchased from National centre of cell science, Pune. These cells were grown in Dulbecco's modified eagle medium (DMEM) enriched with fetal bovine serum (10% v/v) and Penicillin/streptomycin/amphotericin B antibiotic (1% v/v) solution at 37 °C in a humidified 5% CO_2 atmosphere. The media was changed every 2 days. All chemicals used in the cell culture experiment were purchased from Sigma Aldrich. All the cytocompatibility studies were performed in triplicate and results are shown as average.

2.3.7.2. Cells seeding on 3D self-assembled nanofibrous construct

The test samples were cut into specific size and were then sterile by treating with 70% ethanol for 15 min, followed by washing with DMEM media and dried under laminar air flow. The dried samples were further exposed to UV radiation under laminar air flow.[19] The sterile samples were placed in 98 well tissue culture plates. For cell adherence and proliferation study approximately 20000 cells were seeded onto each sample per well and allowed to incubate at 37 °C in a humidified atmosphere containing 5% CO_2. The cell seeded constructs were monitored after 1, 3, and 5 days of incubation.

2.3.7.3. Cell adherence and morphology by fluorescence microscopy

Fluorescence microscopy of stained cells was performed to elucidate the time dependent spreading of L929 cells seeded on self-assembled nanofibrous constructs (20% STNF). DAPI (4′,6-Diamidino-2-phenylindole) and FITC-conjugated phyllodin dyes were used for visualization of the nucleus and cytoskeleton, respectively. After 1, 3, and 5 days of incubation, cells seeded construct were washed with PBS (1X) and fixed in 3% paraformaldehyde in PBS (1X) for 5 min and add 0.5 mL of 0.2% Triton X-100 in PBS to permeabilize the cells. Cells were stained using DAPI (1 μg/mL) and FITC-conjugated phyllodin (3 μg/mL) for 30 min in dark.[20] The cells seeded construct were washed with PBS twice and mount between cover slip and glass slide using a drop of glycerine. Stained cells seeded on constructs were imaged using fluorescence microscope (Zeiss, Axio Imager 2).

MTT assay is a calorimetric technique generally used to check mitochondrial activity. This method is based on the fact that yellow color MTT is reduced to violet color formazan crystal by the action of mitochondrial dehydrogenase so it gives the direct indication about cells viability. Approx 100 μL of MTT (5 mg mL^{-1}) diluted in PBS (1:10) was added to each well, followed by incubation for 4 h at 37 °C in dark. After incubation, the violet formazan crystals were dissolved in 1 mL of dimethyl sulfoxide. The absorbance value of formazan solution was measured at 595 nm in a Bio-Rad microplate reader.

Viability of cells grown on nanofibrous samples was evaluated by Trypan blue dye exclusion assay. The method is based on concept that viable cells exclude the dye so have clear cytoplasm, whereas due to the absorption of dye dead cells have blue cytoplasm.[20]

2.3.8. *In vitro* biodegradation

In vitro biodegradation of nanofibrous sample was assessed using the protocol given by Kasoju *et al.*[21] with some modifications. Pre-dried 20% STNF samples were cut in specific size and weighed. The samples were immersed in 2 mL of PBS with and without trypsin (1 mg/mL from bovine pancrease X3, activity 2500 NFU/mg) and allowed to incubate at 37 °C. To maintain the activity of enzyme, enzymatic solution was replaced every day. At pre determined time point samples were removed from PBS and enzymatic solution washed with distilled water and dried in oven at 60 °C and measured the weight of each samples again. The extent of biodegradation of samples at different time point was determined by the equation:

$$\text{Weight loss (\%)} = \frac{W_o - W_t}{W_o} \times 100 \quad (5)$$

where, W_o is initial mass *i.e.* mass of sample before biodegradation and W_t is mass of sample after biodegradation.

2.3.9. Statistical analysis

The data are presented as mean±SD. One-way ANOVA was performed to assess the experimental data at the statistical significance level of $p<0.05$.

3. Results and discussion

3.1. Characterization of nanofibers

3.1.1. Effect of tasar fibroin concentration

Concentration plays a very important role in electrospinning of polymer solution. At very low concentration jet breaks before reaching collector during stretching under electrostatic force due to insufficient entanglements between polymer molecules that result in bead formation. It is reported that electrospun nanofibers cannot be prepared with mulberry silk/formic acid solution having concentration below 5% (w/v).[20] We found that when the concentration of tasar solution was 10% w/v nanofibers easily deposited at collector plate but when the concentration of tasar fibroin increases to 15% w/v, the self-assembly phenomena appeared. This may be due to the fact that nanofiber jet has relatively higher polymer content which results in fast drying of nanofibers during stretching so relatively dry fibers are deposited on the collector plate. Further increase in concentration of tasar fibroin up to 20% w/v results in deposition of completely dried nanofiber at collector plate and these deposited nanofibers align themselves in electrostatic field forming self-assembly. Figure 2(a)-(c) shows digital photographs of electrospinning process and fiber deposition with varying concentration. It is reported that in the presence of small amount of low molecular weight salt conductivity of polymer solution increases which is prerequisite for initiation of self-assembly. In this case two factors govern the development of self-assembly construct. The first factor is the presence of $CaCl_2$ in dope solution. The low molecular weight salt ($CaCl_2$) gives conductivity to the dope solution which is responsible for self-assembly phenomena (Table 1). During electrospinning, positive potential was given to spinneret and negative potential was given to

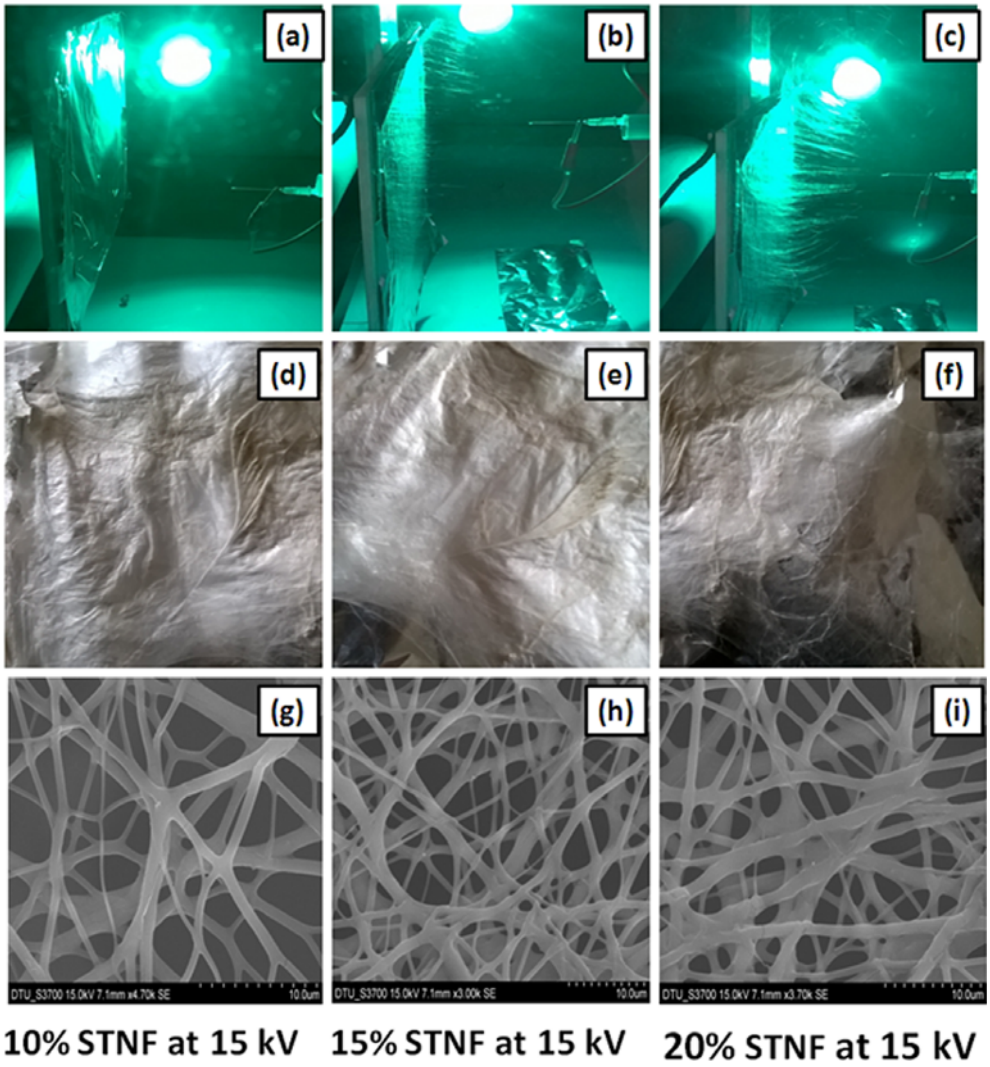

Figure 2. Digital photographs of electrospinning (a) 10% STNF, (b) 15% STNF, and (c) 20% STNF samples, digital photographs of prepared samples (d) 10% STNF, (e) 15% STNF, and (f) 20% STNF sample and SEM images of (g) 10% STNF, (h) 15% STNF, and (i) 20% STNF samples. Where STNF represent 3D self-assembled nanofibrous construct prepared at 10, 15, and 20% w/v tasar fibroin-formic acid/$CaCl_2$ solutions concentration at 15 kV.

collector plate. Positively charged nanofibers jet emerged from the spinneret and travel towards negative charged collector plate. When the positively charged protein nanofibers deposits on the negatively charged collector plate its positive charge discharges through ground plate rapidly due to the presence of $CaCl_2$ and the deposited nanofibers attain overall negative charge of the collector plate. These negatively charged nanofibers further attract positively charged nanofibers jet emerging from spinneret and responsible for self-assembly phenomena[22] which is depicted in schematic representation (Figure 3(a) and (b)).

The second factor responsible of formation of self-assembly construct is the polymer concentration. As the concentration increases, the interaction between the deposited negative nanofibers and incoming positively charged nanofibers jet increases. As the concentration of polymer increases in the dope solution, the relative amount of polymer in the jet is high which results in fast drying of jet during stretching. So, relatively dry nanofibers are deposited on the collector plate and after discharge these fibers attain negative charge of collector plate and tend to attract towards the positively charged spinneret and align themselves in the air. In this way, instead of a 2D nonwoven construct, a highly spongy 3D self-assembled construct formed due to dry spinning of fibers. We found that

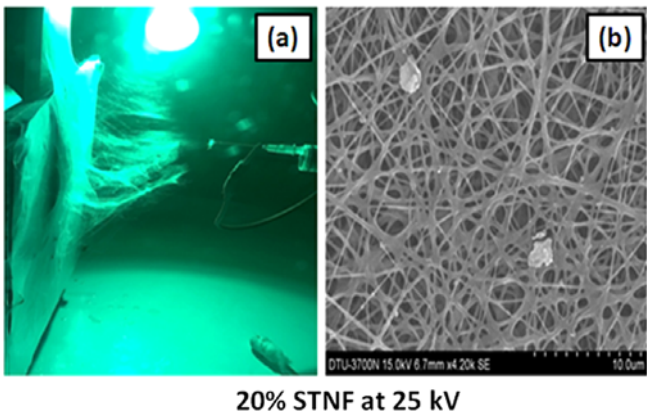

Figure 3. (a) Digital photograph and (b) SEM micrograph of self-assembled tasar nanofibrous mat prepared from 20% (w/v) tasar fibroin-formic acid/$CaCl_2$ solutions at 25 kV.

optimum dry spinning of nanofibers is carried out using 20% w/v solution due to high concentration of tasar protein and low content of fast evaporating solvent. The diameter of nanofiber formed by spinning of solution having concentration of 10% w/v was found to be in the range of 259 to 700 nm with average diameter of 376 nm while diameter of nanofiber was in the range of 310 to 800 nm with average diameter of 533 nm for 15% w/v concentration of solution. The nanofiber mat prepared with 20% w/v tasar formic acid solution has diameter of nanofibers in range of 325 to 880 nm with average diameter of 666 nm. This increase in diameter of nanofibers with concentration is due to the fact that with increase in concentration the amount of polymer in nanofibrous jet increases so it experiences less stretching at fix voltage.

3.1.2. Effect of voltage

With 20% w/v tasar formic acid solution, the average fiber diameter was 666 nm at 15 kV and 8 cm spinneret collector plate distance. When electric potential was increased from 15 to 25 kV, the average diameter of nanofibers was approximately 200 nm (diameter of nanofibers was range from 90 to 250 nm) (Figure 4). With high voltage, the high electrostatic power causes more stretching of jet during flight before reaching collector. In this way a highly spongy, porous 3D self-assembled construct develop by processing of high concentration of tasar protein. On further increasing the voltage, there was no effect on the diameter of the nanofibers.

All the nanofibrous 3D constructs are highly porous in nature. Pore size of nanofibrous 3D constructs was determined by image J software using five different images of same sample. The diameter of pores as determined by image J software was in the range of 200-400 nm. Since we were able to optimized 3D electrospun self-assembled construct with approx 200 nm fiber diameter at 20% protein concentration and 25 kV voltage, further studies are focused on the above construct and the name assigned to this is 20% STNF.

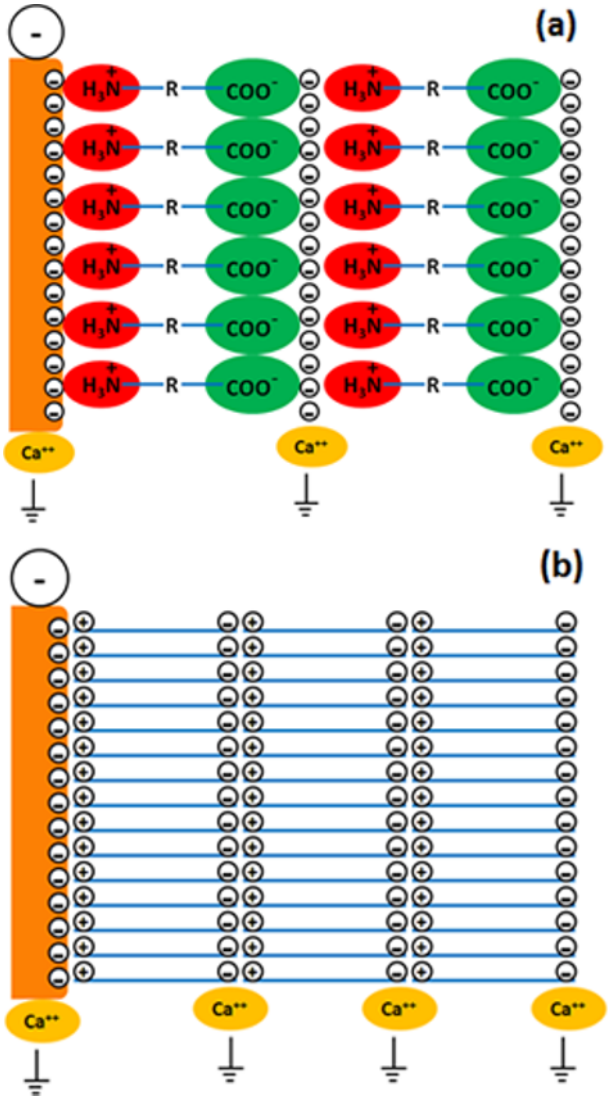

Figure 4. (a) Schematic presentation of self assembly of nanofiber during electrospinning in the presence of low molecular salt. (b) Diagrammatic representation of self assembly of nanofiber during electrospinning in the presence of low molecular salt.

3.2. Structural and swelling behavior of self-assembled nanofibrous mat

Most of the properties of the silk proteins depend on its conformation. During regeneration of fibroin proteins, conformation of silk proteins changes from β-sheet to random coil after dissolution and again from random coil to β-sheet during crystallization process. So, it is very important to analyze conformation of silk proteins before and after spinning. Conformation of tasar fibroin protein after dissolution in ionic liquid, dialyzed tasar

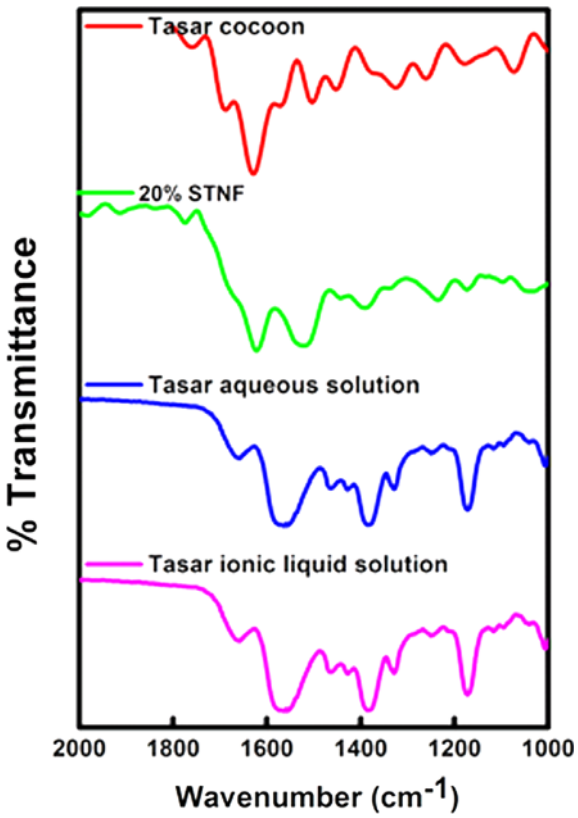

Figure 5. FTIR spectra of tasar solution and self-assembled nanofibrous mat.

fibroin aqueous solution, crystallized tasar 3D nanofibrous construct and degummed tasar cocoon fibroin fiber was analyzed using FTIR and different spectra are shown in Figure 5. FTIR spectrum of tasar fibroin aqueous solution and tasar ionic liquid show similar band pattern. For both, the characteristic protein bands appear at 1652 cm^{-1} (amide I), 1558 cm^{-1} (amide II), and 1252 cm^{-1}, are characteristic of random coil conformation of fibroin protein. Crystallized nanofiber sample shows band at 1612 (amide I), 1525 (amide II), and 1230 (amide III) cm^{-1} are characteristic of β-sheet. The random coil conformation of tasar aqueous solution has changed to β-sheet conformation after electrospinning, as these electrospun constructs were crystallized in methanol after spinning. Natural degummed tasar cocoon fiber shows characteristic bands correspond to β-sheet conformation similar to crystallized nanofibrous construct except one peak at 1690 cm^{-1} which indicate existence of trace of α-helical structure in degummed natural tasar cocoon fibers.

3.3. Physico-chemical and mechanical properties of 3D self-assembled nanofibrous construct

Figure 6 shows water uptake behavior of 20% STNF over time. Water absorbance capacity of 20% STNF increases with time and attains equilibrium after 48 h. The maximum water uptake capacity of 20% STNF was found to be 115% which is higher than 2D tasar fibroin nanofibers mat reported in literature.[23] Bhattacharjee *et al.*[23] prepared tasar gland protein/PVA blend based nanofibers and observed that with increase in tasar fibroin content in PVA solution the swelling ability of nanofibrous mat had increased to a maximum value of 92%. The high water uptake capacity is very important for absorption of exudates and provide moist environment that allow the moist healing of wounds by stimulating growth and regeneration of neo-tissues.

Porosity measurement for a material to be used for biomedical and tissue engineering application is very important because a porous matrix provides high surface area which allows the migration of essential metabolites and biomolecules that is required for growth of cells and allow passage of water vapor and exchange of gases. The maximum porosity of 3D self-assembled tasar nanofibrous construct obtained by liquid displacement was found to be 85% (Table 1), which is slightly higher as compared to the 2D eri-tasar nanofibrous mat (79%) prepared by Panda *et al.*[24] AFM images of optimized self-assembled nanofibrous mat also showed highly porous and interconnected architecture having average diameter of nanofiber about 200 nm (Figure 7) which is in good agreement with size obtained by SEM. The nanophase roughness of self-assembled nanofibrous mat was found to be 10.48 nm, which would be very advantages for adherence of seeded fibroblast cells.

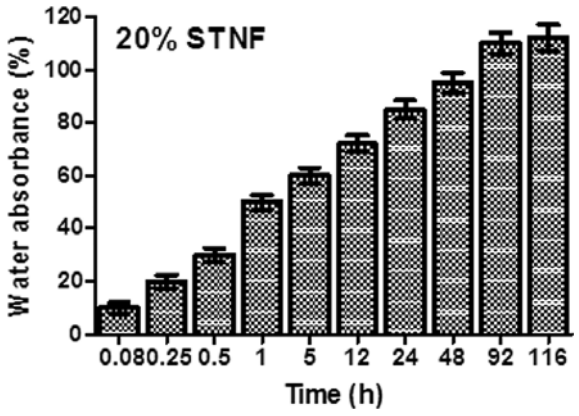

Figure 6. Water uptake behavior of self-assembled nanofibrous mat.

A good water vapor transmission rate is prerequisite for a material to be used for wound dressing due to the fact that low water vapor causes buildup of exudates while high water vapor transmission rate causes dehydration. Water vapor transmission rate of 20% STNF is 2500 $g/m^2/day$ which would be favorable for third degree wound. The value found in this case is higher with the value reported in literature for pure muga nanofibrous mat (2250 $g/m^2/day$)[14] and muga/PVA nanofibrous mat (2330 $g/m^2/day$).[25] The WVTR value of pure tasar nanofibrous is not reported till date.

Mechanical properties of 20% STNF were also determined. Mechanical properties of a material to be used as wound dressing or skin tissue scaffolds should be optimum as higher mechanical strength results in development of stress on growing tissue and lower mechanical strength would result in failure of tissue engineering construct. Besides, good physico-chemical and biological properties, appropriate elasticity and toughness are also prerequisite condition for wound dressing materials especially when it is used in load bearing area such as knee point and elbow. Table 2 shows the mechanical properties of 20% STNF. The tensile strength and elongation value for 20% STNF sample was found to be 8 MPa and 12 mm, respectively. The tensile strength of the 3D self-assembled tasar fibroin construct is significantly (p<0.05) higher than that of eri-tasar blend nanofibous 2D mat (1.8 MPa) prepared by Panda *et al.*[24] The mechanical integrity of 20% STNF is in close agreement with that of human skin (5 to 30 MPa)[26,27] and cell derived skin graft (713 kPa).[28]

3.4. Cytocompatibility of 3D self-assembled tasar nanofibrous mat

Dermal fibroblast cells play an important role in regeneration of damage tissue. Scaffolds provide template for growth and proliferation of seeded cells so it is very important that scaffolds should be highly porous, biocompatible that could facilitate adherence, proliferation and migration of cells. So, the suitability of these highly porous and spongy nanofibrous web towards regenerative medicine as skin graft was assessed

Table 1. Conductivity of formic acid/$CaCl_2$ and its silk solution

Samples	Formic acid (98%)	Formic acid/$CaCl_2$ (2%w/v) solution	10% Silk formic acid/ $CaCl_2$ solution	15% Silk formic acid/ $CaCl_2$ solution	20% Silk formic acid/ $CaCl_2$ solution
Conductivity (μS/cm)	1070	1161	1240	1523	1611

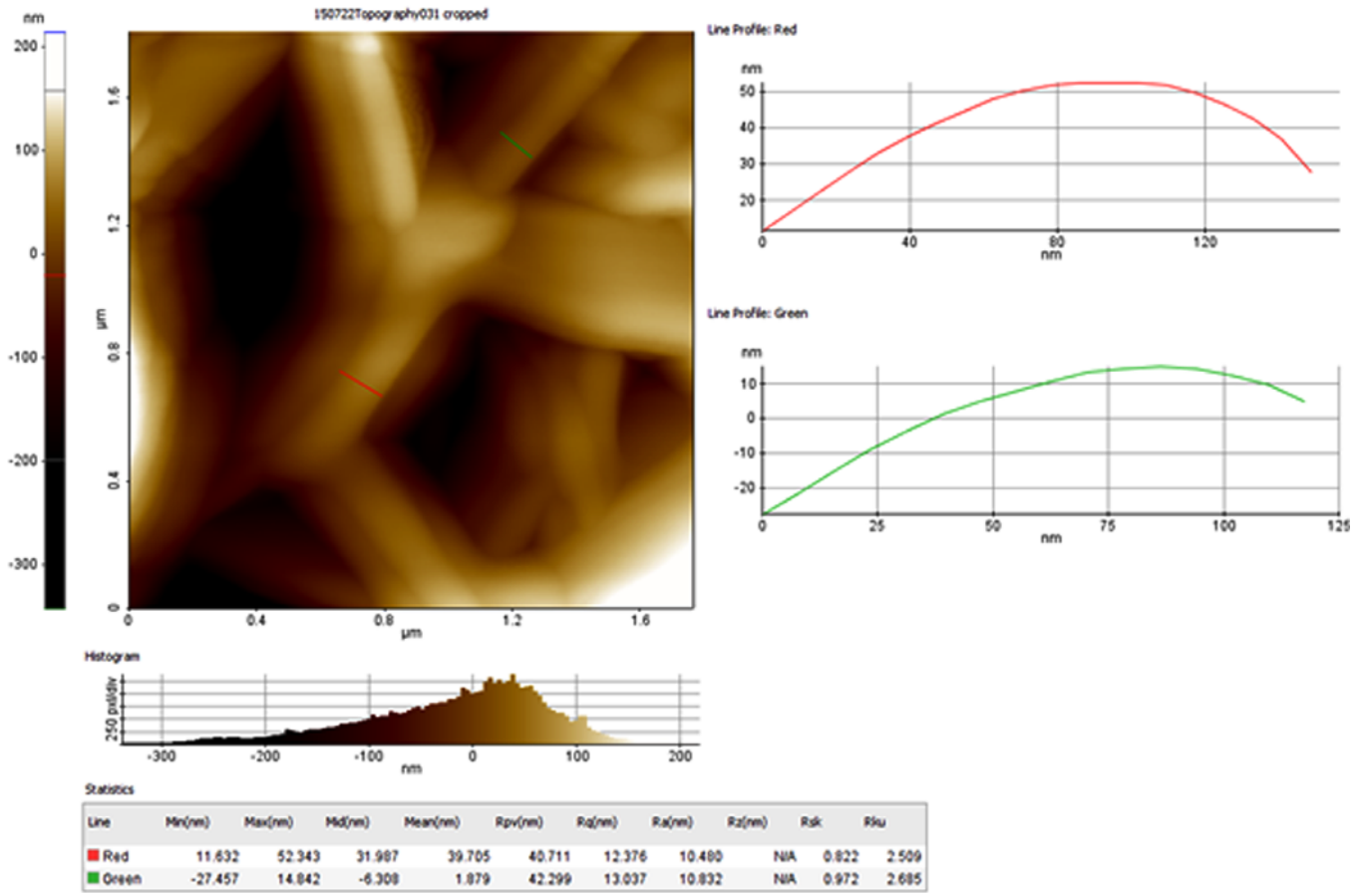

Figure 7. AFM image of 3D self-assembled tasar nanofibrous mat (20% STNF).

Table 2. Physico-chemical and mechanical properties of 3D self-assembled nanofibrous construct. Data are represented as mean±SD for n=3

Samples	Tensile strength (MPa)	Elongation at Break (mm)	Porosity (%)	Water uptake (%)	WVTR (g/m^2/day)	Nanophase Roughness (R_a)
20% STNF	8±0.1	12±0.4	85±2	115±5	2500±50	10.48

using L929 skin fibroblast cells.

The viability of L929 fibroblast cells seeded on self-assembled nanofibrous mats was accessed through MTT assay. MTT assay is a calorimetric technique related to metabolic activity of cells and is based on the fact that yellow formazan dye reduces to violet color crystal by the action of mitochondrial dehydrogenase giving information about viability of cells. Figure 8(a) showed that absorbance value formazan solution increased with time of incubation for self-assembled nanofibrous mat and there was no significant difference (p>0.05) in absorbance value between self-assembled nanofibrous mat and tissue culture plate (TCP) after 5 days of incubation.

Adherence growth and spreading of cells seeded on self-assembled nanofibrous mat was increased with time of incubation. Figure 8(b) shows that number of cells seeded on self-assembled nanofibrous mat significantly increased (p<0.05) after 5 days of incubation and it was comparable to tissue culture plate (p>0.05).

The proliferation and spreading of L929 fibroblast cell seeded on 3D self-assembled nanofibrous mat were assessed through fluorescence microscopy that is depicted in Figure 8(c). Fluorescence microscopic images of DAPI stained cells showed that nuclei adhered to the surface of nanofibrous mat after 1 day of incubation and nuclear density increase with time of incubation and there was no significant difference in nuclear density found for TCP and nanofibrous mat (p>0.05) suggesting the normal growth of cells on film over the period of 5 days. Fluorescence images of FITC conjugated phyllodin stained cells clearly showed that cytoskeleton of L929 fibroblast cells completely attain their normal morphology after 1 day of incubation. So, it is clear from proliferation assay that the number of cells increased with time of incubation and there was no any significant difference found between cells density obtained for nanofibrous mat and TCP after 5 day of incubation (p>0.05).

The higher growth and proliferation of cells seeded on this spongy self-assembled nanofibrous mats were related to its architecture and morphology. The high surface area and interconnected porous morphology of this web like nanofibrous mats mimic architecture of natural extracellular matrix and provide favorable environment that facilitate high water absorbance, ease permeation of water vapor, exchange of gases, transportation of essential nutrients and metabolites required for growth of cells which favor adherence and proliferation of seeded cells for the development of tissue engineering construct. Besides

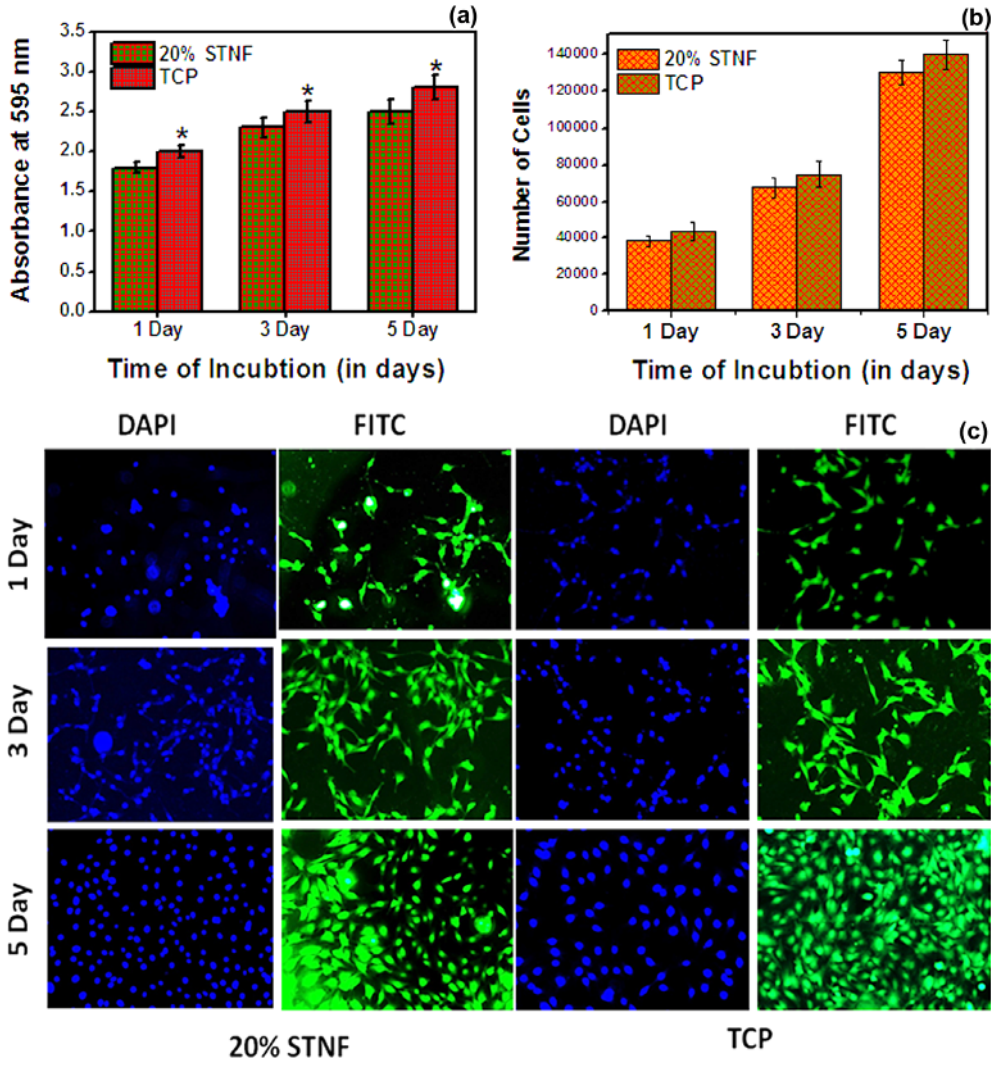

Figure 8. (a) MTT assay of L929 cells seeded on 3D self-assembled nanofibrous mat over the time of incubation. Experiments are performed in triplicate. Data are presented as mean±SD. (b) Number of L929 cells proliferated on the 3D self-assembled nanofibrous mat over the time of incubation. Experiments are performed in triplicate. Data are presented as mean±SD. (c) Fluorescence images (stained with DAPI and FITC-conjugated phalloidin) of L929 cells seeded 3D self-assembled nanofibrous mat.

the porous architecture, higher surface area and nanophase surface roughness, the higher cell adherence and proliferation is also due to the presence of Arg(R)-Gly(G)-Asp(D), a positive charge residue which is also responsible for integrin mediated cells adherence.

Adherence, proliferation and viability of cells seeded on this 3D self-assembled spongy nanofibrous mat suggest good biocompatibility of this matrix and it would be a good candidate as a tissue engineered construct for tissue engineering and regenerative medicine and it hold good agreement with the findings reported earlier for nonmulberry based constructs such as 3D scaffolds, aerogels and cryogels.[26-31]

3.5. *In vitro* biodegradation

The biodegradation of a material to be used as wound dressing should be optimum *i.e.* degradation of materials should match with regeneration of neo-tissues because a slow rate of biodegradation imposes stress on developing tissue while fast degradation results in development of exudates beneath the dressing. *In vitro* biodegradation of the 20% STNF was evaluated by protocol reported earlier.[14,21] *In vitro* biodegradation of 20% STNF was investigated by determining the mass remained during the incubation in PBS with and without trypsin (Figure 9). 20% STNF samples showed a controlled rate of degradation up to the value of 6% in PBS over 30 days of incubation. The enzymatic degradation of 20% STNF was significantly higher as compared to non-enzymatic PBS biodegradation up to 30 days of incubation. After 30 days of incubation in trypsin enzyme, 20% STNF showed higher biodegradation 63%. It is also reported that in protease XIV medium eri/tasar blend nanofibers 2D mat degrade up to 26% within 24 h.[32] We also found that tasar fibroin cast films showed only 51% degradation after 30 days of trypsin mediated biodegradation. The higher biodegradation of 20% STNF as compared to cast film is due to the fact that nanofibrous 3D construct has higher surface area and porosity as compared to cast films that result in higher interaction of materials surface with enzyme.

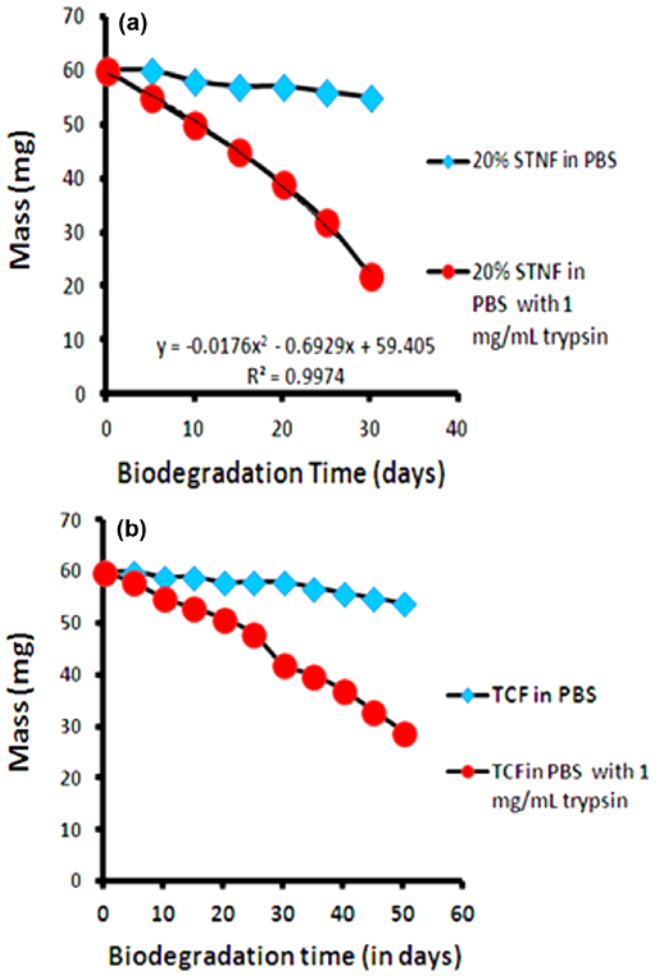

Figure 9. *In vitro* biodegradation of (a) 20% STNF and (b) tasar cast film after 30 days of incubation.

4. Conclusions

An effort has been made to develop highly porous 3D self-assembled tasar nanofibrous mat to improve the efficacy of tasar proteins for skin tissue engineering and regenerative medicine. These 3D self-assembled tasar nanofibrous mats show good water uptake capacity, water vapor transmission rate and biocompatibility that would be potential material for skin tissue engineering and regenerative medicine. Tasar silk fibroin protein extracted from cocoon is successfully regenerated in the form self-assembled 3D nanofibrous construct, that would open a new facile way for the fabrication of nonmulberry silk fibroin based therapeutic devices, drug delivery vehicles and scaffolds but still there is a need to check efficacy of the prepared matrix toward *in vivo* behavior for commercial applications.

References

(1) V. Falanga, *Wound Repair Regen.*, **8**, 347 (2000).
(2) T. A. Mustoe, K. O'Shauqhnessy, and O. Kloeters, *Plast. Reconstr. Surg.*, **117**, 35S (2006).
(3) K. A. Rieger, N. P. Birch, and J. D. Schiffman, *J. Mater. Chem. B*, **1**, 4531 (2013).
(4) C. M. Srivastava and R. Purwar, *J. Appl. Polym. Sci.*, **134**, 1 (2017).
(5) A. Formhals and R. S. Gastell, US1975504 A (1934).
(6) B. Sun, Y. Z. Long, F. Yu, M. M. Li, H. D. Zhang, W. J. Li, and T. X. Xu, *Nanoscale*, **4**, 2134 (2012).
(7) M. Li and Y. Long, *Mater. Sci. Forum*, **688**, 95 (2011).
(8) H. Okuzaki, T. Takahashi, N. Miyajima, Y. Suzuki, and T. Kuwabara, *Macromolecules*, **39**, 4276 (2006).
(9) B. Sun, Y. Z. Long, H. D. Zhang, M. M. Li, J. L. Duvail, X. Y. Jiang, and H. L. Yin, *Prog. Polym. Sci.*, **39**, 862 (2014).
(10) C. Acharya, S. K. Ghosh, and S. C. Kundu, *Acta Biomater.*, **5**, 429 (2009).
(11) N. Panda, A. Biswas, L. B. Sukla, and K. Pramanik, *Appl. Biochem. Biotechnol.*, **174**, 2403 (2014).
(12) P. Bhattacharjee, B. Kundu, D. Naskar, T. K. Maiti, D. Bhattacharya, and S. C. Kundu, **103**, 271 (2015).
(13) H. Zhao, X. Ren, Y. Zhang, and L. Huang, *Bio-med Mater. Eng.*, **26**, S89 (2015).
(14) C. M. Srivastava and R. Purwar, *Mater. Sci. Eng. C*, **68**, 276 (2016).
(15) B. B. Mandal and S. C. Kundu, *Biomaterials*, **30**, 2956 (2009).
(16) E. S. Gadelmawla, M. M. Koura, T. M. Maksoud, M. Elewal, and H. H. Soliman, *J. Mater. Process Technol.*, **123**, 133 (2002).
(17) S. E. Wharram, X. Zhang, D. L. Kaplan, and S. P. McCarthy, *Macromol. Biosci.*, **10**, 246 (2010).
(18) Z. Pei, Q. Sun, X. Sun, Y. Wang, and P. Zhao, *Biomed. Mater. Eng.*, **26**, S111 (2015).
(19) M. A. Moraes, R. F. Weska, and M. M. Beppu, *J. Biomed. Mater. Res. B: Appl. Biomater.*, **102**, 869 (2014).
(20) J. Ayutsede, M. S. Gandhi, M. Sukigara, H. E. Micklus, and F. K. Chen, *Polymer*, **46**, 1625 (2005).
(21) N. Kasoju, R. R. Bhonde, and U. Bora, *J. Tissue Eng. Regen. Med.*, **3**, 539 (2009).
(22) X. Wang, K. Zhang, M. Zhu, H. Yu, Z. Zhou, Y. Chen, and B. S. Hsiao, *Polymer*, **49**, 2755 (2008).
(23) P. Bhattacharjee, B. Kundu, D. Naskar, T. K. Maiti, D. Bhattacharya, and S. C. Kundu, *Biopolymers*, **103**, 271 (2015).
(24) N. N. Panda, A. Biswas, K. Pramanik, and S. Jonnalagadda, *J. Biomed. Mater. Res.*, **103**, 971 (2015).
(25) D. Chouhan, B. Chakraborty, S. K. Nandi, and B. B. Mandal, *Acta Biomater.*, **48**, 157 (2017).
(26) B. B. Mandal and S. C. Kundu, *Macromol. Biosci.*, **8**, 807 (2008).
(27) Y. Zhang and S. J. Park, *J. Polym. Sci. B*, **55**, 1890 (2017).
(28) R. R. Mallepally, M. A. Marin, V. Surampudi, B. Subia, R. R. Rao, S. C. Kundu, and M. A. McHugh, *Biomed. Mater.*, **10**, 035002 (2015).
(29) B. Kundu and S. C. Kundu, *Biomed. Mater.*, **8**, 55003 (2013).
(30) J. Pan, N. Liu, H. Sun, and F. Xu, *PLoS One*, **9**, e112885 (2014).
(31) J. E. W. Ahlfors and K. L. Billiar, *Biomaterials*, **28**, 2183 (2007).
(32) N. Panda, A. Biswas, L. B. Sukla, and K. Pramanik, *Appl. Biochem. Biotechnol.*, **174**, 2403 (2014).

